JOURNAL OF MATERIALS SCIENCE 22 (1987) 3185–3193

Crystallization behaviour and mechanical properties of polypropylene-based composites

MAURIZIO AVELLA, EZIO MARTUSCELLI, CLAUDIO SELLITTI, ENEA GARAGNANI*
*Istituto di Ricerche su Tecnologia dei Polimeri e Reologia del CNR, Via Toiano 6, 80072 Arco Felice, Napoli, Italy and *Himont Centro Ricerche "G. Natta", Ferrara, Italy*

The influence of glass fibres on the primary nucleation process, isothermal radial growth rate of spherulites and overall kinetic rate constant of isotactic polypropylene (iPP) has been examined. The polypropylene was also modified by means of acrylic acid (iPP*) in order to improve the adhesion between the matrix and the fibres, and the relative properties were compared with those concerning the composites having as matrix plain iPP. Moreover the mechanical properties of injection-moulded composites containing iPP and iPP* have been studied. These properties improved on increasing the fibre content. It was found that for the same glass-fibre content better values of the elongation at break and creep are observed in the case of reinforced polypropylenes having as matrix acrylic acid modified polypropylene.

1. Introduction

Thermoplastic polymers such as isotactic polypropylene (iPP) are often reinforced by using glass fibres in order to increase the stiffness, tensile strength and dimensional stability at elevated temperatures [1, 2]. The properties of a glass-reinforced polypropylene (GRiPP) are greatly dependent on the adhesion between the matrix and the fibres and then on the interface structure. Usually the interfacial bond strength between the fibres and the matrix is enhanced by using a fibre surface treatment by means of silane coupling agents. In some reinforced crystallizable thermoplastics it has been found that the fibres, acting as nucleating agents, cause an epitaxial crystallization of the matrix polymer [3, 4].

In the present paper we report the results of an investigation concerning mainly the following topics:

(i) The study of the influence of glass fibres on the primary nucleation process, on the isothermal radial growth rate and on the overall kinetic rate constant of iPP.

(ii) The study of the influence of a modified polypropylene, obtained by reaction with acrylic acid, on the adhesion between the matrix and the fibres and on the crystallization process.

(iii) The study of the properties of injection-moulded samples in order to find relationships between the nature of the matrix, the fibreglass content and the fibre–matrix adhesion.

2. Experimental procedure

2.1. Materials

The samples investigated together with their codes are described in Table I. The samples, supplied by Centro Ricerche Giulio Natta, Himont (Ferrara, Italy) were obtained by using a Bandera type of extruder (ϕ = 30 mm). An extrusion temperature of 190° C for homopolymers and 220° C for reinforced materials was used. The components of the formulated samples were as follows:

(i) isostatic polypropylene (iPP) ($\overline{M_n}$ = 58 000, $\overline{M_w}$ = 275 000, $\overline{M_w}/\overline{M_n}$ = 4.74; melt index = 10 g

TABLE I Description of the samples investigated and their codes

Sample No.	iPP (%)	Acrylic acid modified iPP, IPP* (wt %)	Sodium benzoate (wt %)	Glass fibres (wt %)	Code*
1	100	–	–	–	iPP-1
2	90	–	–	10	GRiPP-2
3	30	–	–	20	GRiPP-3
4	70	–	–	30	GRiPP-4
5	90	10	–	–	iPP–iPP*-5
6	81	9	–	10	GRiPP–iPP*-6
7	72	8	–	20	GRiPP–iPP*-7
8	63	7	–	30	GRiPP–iPP*-8
9	99.70	–	0.30	–	NiPP-9
10	89.73	–	0.27	10	GRNiPP-10
11	79.76	–	0.24	20	GRNiPP-11
12	69.79	–	0.21	30	GRNiPP-12

iPP = plain isotactic polypropylene, iPP = iPP modified with acrylic acid, GR = glass reinforced, N = nucleated.

0022–2461/87 $03.00 + .12

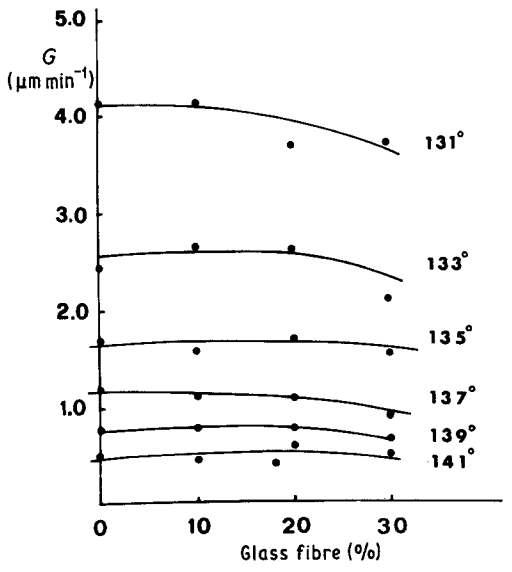

Figure 1 Radial growth rate of spherulites G against the glass fibre content at constant temperature of crystallization T_c (° C) for iPP homopolymer and GRiPP samples.

per 10 min. The iPP was prepared using a Ziegler–Natta third generation high yield supported catalyst system (super-active catalysts);

(ii) acrylic acid modified isotactic polypropylene (iPP*) obtained by melt-mixing the iPP with 2% by weight of acrylic acid at $T = 190°$ C;

(iii) sodium benzoate: this component was used as nucleating agent (0.3% by weight);

(iv) glass fibres CP713 supplied by Vitrofil S.p.A. (Vado Ligure, Italy). These fibres are constituted of Type E glass coated with a γ-amine propyltriethoxysilane, a coupling agent particularly indicated for polypropylene matrices.

2.2. Nucleation and growth of spherulites by optical microscopy (OM)

A Reichert polarizing optical microscope equipped with a Mettler hot stage was used for studying the nucleation and the radial growth rate (G) of spherulites isothermally crystallized at different crystallization temperatures (T_c).

The nucleation studies were carried out by utilizing microtomed sections of 25 μm thickness. The radial growth rate of spherulites was determined on films obtained by melt-squeezing part of the samples between a microscope slide and a cover glass.

The following procedure was used: the sample was heated at 190° C and kept at this temperature for 5 min to destroy any traces of crystallinity, then the temperature was rapidly lowered to a prefixed T_c and the sample allowed to crystallize isothermally. The radial growth of a spherulite was monitored during crystallization, taking photomicrographs at appropriate intervals of time. From the measured radius (r), plotted against the time (t), the radial growth rate (G) was calculated as the slope of the resulting straight lines.

2.3. Overall kinetic rate constant by differential scanning calorimetry (DSC)

The kinetics of isothermal crystallization from the melt was studied by using a Mettler TA-3000 differential scanning calorimeter operating under N_2 atmosphere. The following procedure was employed: the samples were kept for 5 min at 190° C and then rapidly cooled to the crystallization temperature T_c.

The heat (dH/dt) evolved during the isothermal crystallization was recorded as function of time t and the weight fraction X_t of material crystallized after the time t was determined from the relation

$$X_t = \int_0^t (dH/dt)\,dt \Big/ \int_0^\infty (dH/dt)\,dt$$

where the first integral is the crystallization heat evolved at the time t and the second integral is the total crystallization heat for $t = \infty$.

The melting temperature T'_m and the apparent enthalpy of fusion ΔH_f^* of each sample after isothermal crystallization at T_c were calculated from DSC

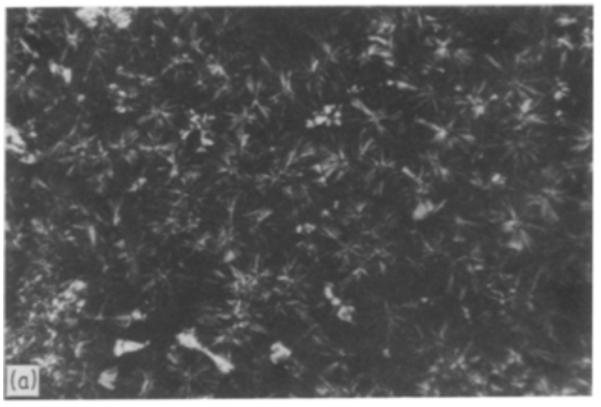

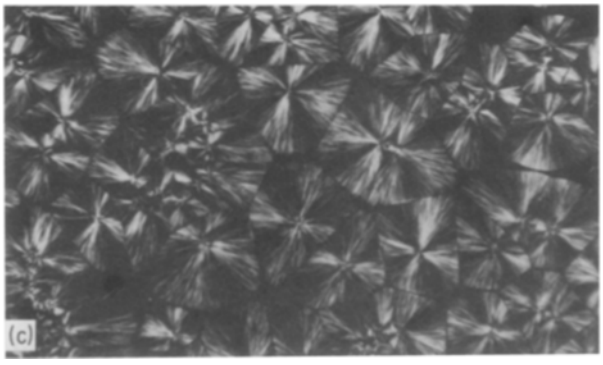

Figure 2 Optical micrographs of melt-crystallized films of iPP-1: T_c = (a) 129, (b) 135, (c) 139° C.

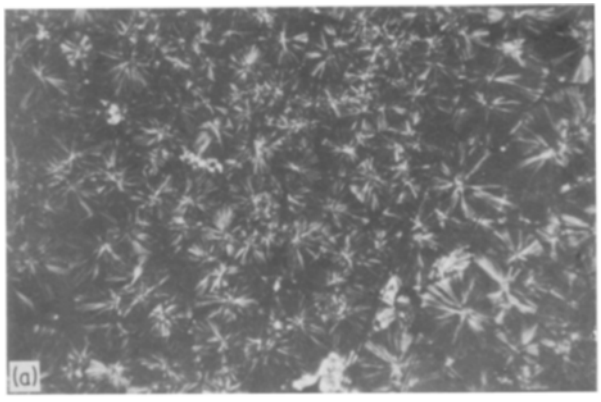

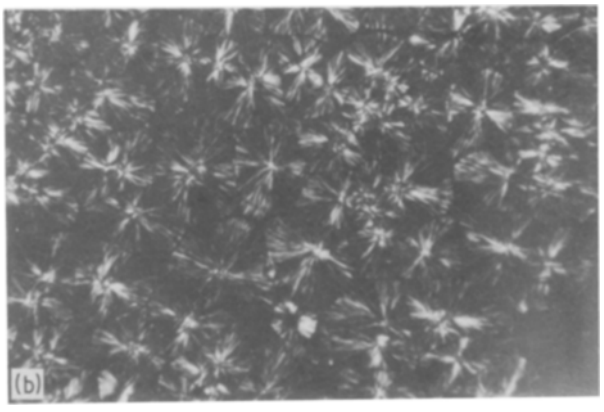

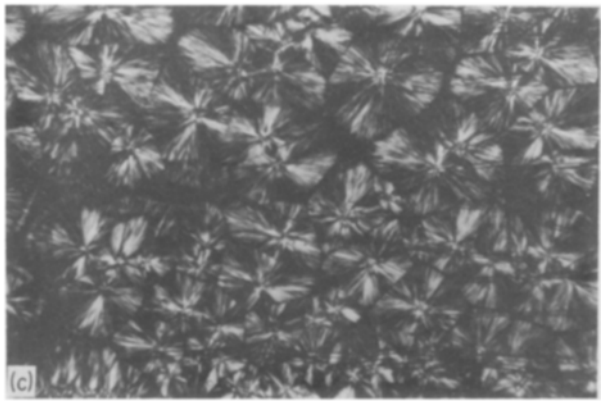

Figure 3 Optical micrographs of melt-crystallized films of GRiPP-2: T_c = (a) 129, (b) 135, (c) 139° C.

endotherms obtained by heating the samples directly from T_c to T'_m with heating rate of 20 (° C) min^{-1}.

The temperature of the calorimeter was calibrated against the melting points of high-purity standards under different heating conditions with a precision of $\pm 0.2°$. The crystallinity fraction X_c of the samples was determined at each T_c by the ratio of ΔH_f^* to the fusion enthalpy of a sample of iPP with 100% crystallinity, taken as 50 kcal kg^{-1} (209 kJ kg^{-1}) [5].

2.4. Scanning electron microscopy (SEM) analysis

The adhesion and morphological investigations were carried out by using a Philips 501 SEM on fracture surfaces obtained by tensile breakage. The samples for SEM observations were metallized by means of a Polaron sputtering apparatus with Au–Pd alloy.

2.5. Mechanical properties

The mechanical behaviour was studied on samples obtained by injection moulding. Moulding temperatures of 190 and 250° C were used for non-reinforced and reinforced samples, respectively. The pressure in the mould was 10 kg cm^{-2}.

Tests were performed according to ASTM standard methods.

3. Results and discussion

3.1. Spherulite radial growth rate

The trend of radial growth rate of spherulites (G) against the glass-fibre content at constant crystallization temperature (T_c) for iPP homopolymer and GRiPP samples (Samples 1 to 4 in Table I) is shown in Fig. 1.

From the figure it emerges that, for a given sample, G decreases with an increase of T_c; moreover it seems that the presence of glass fibres, especially at low

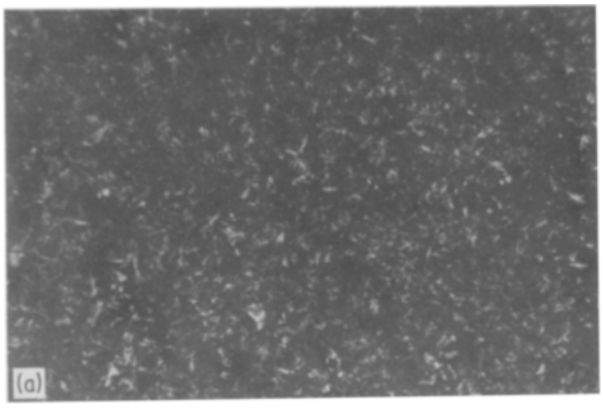

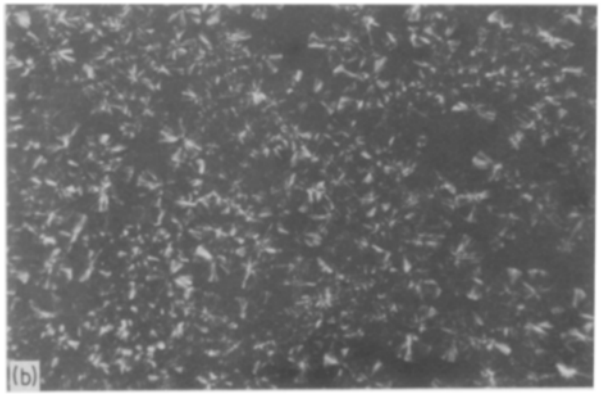

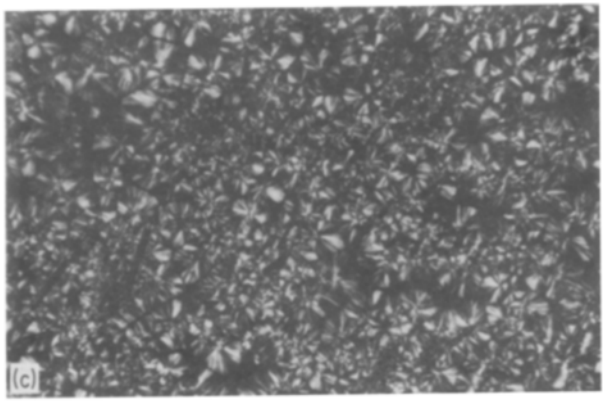

Figure 4 Optical micrographs of melt-crystallized films of GRiPP-3: T_c = (a) 129, (b) 135, (c) 139° C.

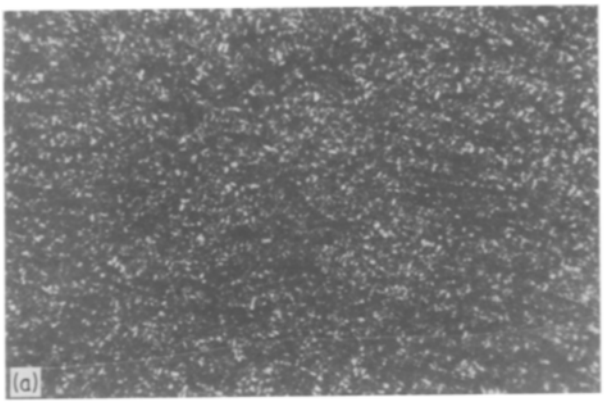

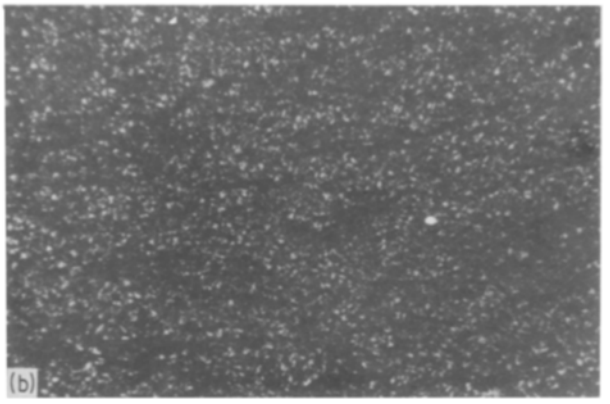

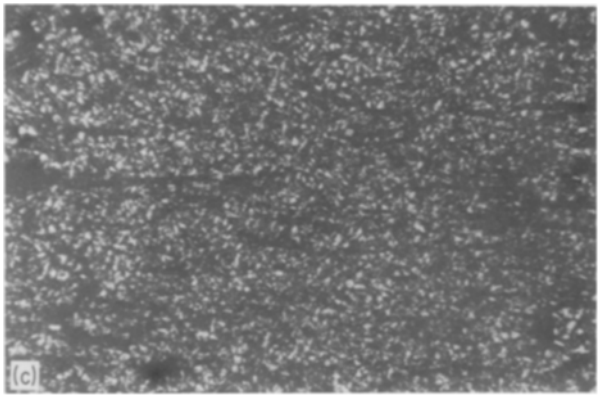

Figure 5 Optical micrographs of melt-crystallized films of GRiPP-4: T_c = (a) 129, (b) 135, (c) 139° C.

undercooling, does not significantly influence G. A slight decrease in G is observed only at very high undercooling and at higher fibre content. Optical photomicrographs of thin films of iPP and GRiPP samples crystallized at different temperatures (129–135–139° C) are shown in Figs 2 to 5. From a comparison of the photomicrographs it clearly emerges that the glass fibres determine a strong nucleating effect as evidenced by the fact that the average dimensions of iPP spherulites are comparatively lower in GRiPP samples.

This effect is more accentuated in samples with higher glass fibre content (see Fig. 5). No formation of transcrystalline regions between glass fibres and matrix interface is observed. In the case of samples containing iPP* and nucleating agents the crystallization leads to microspherulites, thus no G measurements were possible.

3.2. Overall kinetics of crystallization

The half-time of crystallization $t_{0.5}$ for the plain iPP and GRiPP samples (Samples 1 to 4) and for iPP–iPP* and GRiPP* composites (Samples 5 to 8) is shown as a function of T_c in Figs 6 and 7, respectively.

From an examination of the trends of the curves the following emerges:

(i) In the case of iPP and GRiPP (Samples 1 to 4), the values of $t_{0.5}$ for a given T_c decrease with an increase of glass fibre content. This fact is in agreement with Equation 1 that links the overall kinetic rate constant K_n with the spherulite growth rate G and the nucleation density $\bar{N}$ [6]:

$$K_n = \frac{4\pi\varrho_c}{3\varrho_a(1 - \lambda_\infty)} G^3 \bar{N} \qquad (1)$$

with

$$K_n = \frac{\ln 2}{t_{0.5} n} \qquad (2)$$

where ϱ_a and ϱ_c are the density of amorphous and crystalline phases, respectively, λ_∞ is the overall crystallinity at the time $t = \infty$ and n is an Avrami exponent. As the density of nucleation increases with an increase of glass fibre content, whereas the variation of G is practically negligible, the values of $t_{0.5}$ decrease (K_n increases) with an increase of glass fibre content.

(ii) iPP–iPP* and GRiPP–iPP* (Samples 5 to 8) show values of $t_{0.5}$ lower than GRiPP (Samples 1 to 4). Such a finding is accounted for by the predominant nucleating effect of acrylic acid; moreover the $t_{0.5}$ values of reinforced samples (Samples 6 to 8) are

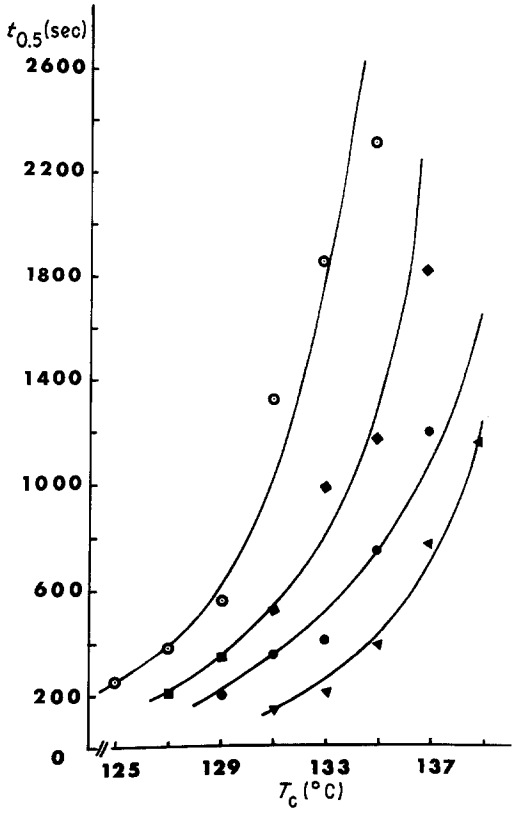

Figure 6 Half-time of crystallization $t_{0.5}$ as a function of crystallization temperature for (⊙) iPP-1, (◆) GRiPP-Z, (●) GRiPP-3, (▲) GRiPP-4.

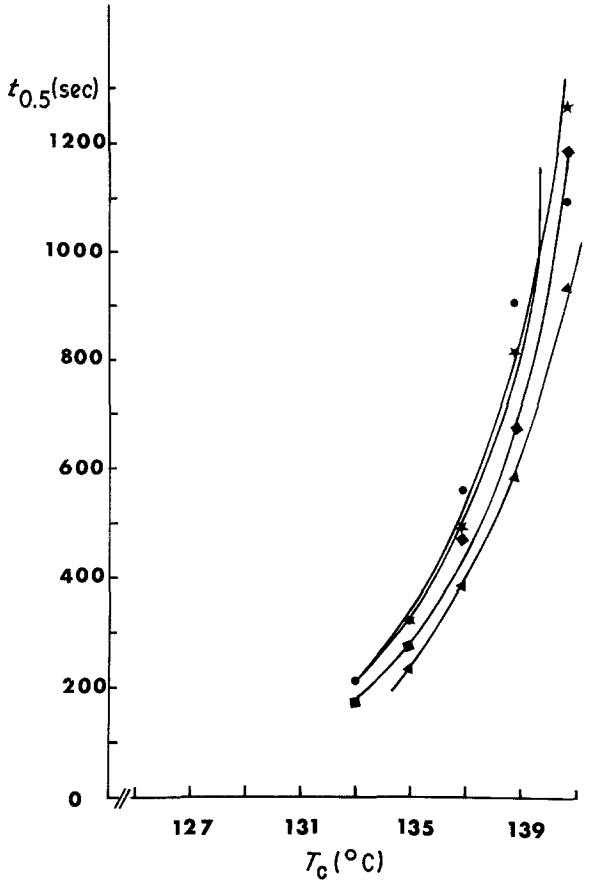

Figure 7 Half-time of crystallization $t_{0.5}$ as a function of crystallization temperature for (▲) iPP–iPP*, (●) GRiPP–iPP*-6, (◆) GRiPP-iPP*-7, (★) GRiPP–iPP*-8.

slightly higher than for the iPP–iPP* sample (see Table II).

Plots of $\log[-\log(1 - X_t)]$ against $\log t$ turn-out to be linear for all samples and T_c investigated, indicating that the kinetics of bulk crystallization follows the Avrami equation [6]:

$$\log[-\log(1 - X_t)] = \frac{1}{2.3}\log kn + n \log t \quad (3)$$

In Equation 3 X_t is the weight fraction of crystallizable material crystallized at time t, n is the Avrami exponent and K_n is the overall kinetic rate constant. The values of n and K_n, obtained from the slopes of the straight lines and from Equation 2, are reported together with $t_{0.5}$ in Table II for all samples examined. The n values vary, for all samples, between 1.8 and 2.9.

3.3. Melting behaviour

The temperature corresponding to the maximum in the DSC endotherms has been assumed to be the apparent melting temperature T'_m of the samples. In agreement with the Hoffman relation [7],

$$T'_m = T_m\left(\frac{\gamma - 1}{\gamma}\right) + \frac{T_c}{\gamma} \quad (4)$$

Straight lines are obtained when the observed melting temperature (T'_m) of iPP, GRiPP and GRiPP–iPP* (Samples 2 to 8) are plotted against the crystallization temperature T_c in Figs 8 and 9. In Equation 4, T_m is the equilibrium melting temperature and γ is a constant that is given by the ratio between the final thickness of the crystalline lamellae and the initial critical thickness.

The value of T_m and γ calculated by extrapolation of the T'_m–T_c lines to the line of equation $T'_m = T_c$ and from the slopes, respectively, are reported for all samples in Table III.

As shown the T_m values for Samples 1 to 4 decrease slightly with the glass fibre content, whereas T_m is constant for the samples containing IPP*. It is interesting to observe that γ is almost constant (between 1.9 and 2.1) for all samples investigated.

3.4. Nucleation control of crystallization rate

Assuming that the growth of lamellae is controlled by

TABLE II Half-time of crystallization $t_{0.5}$, Avrami index n and overall kinetic rate constant K_n of samples as a function of crystallization temperature

T_c	iPP-1 [1]			GRiPP-2			GRiPP-3			GRiPP-4		
	$t_{0.5}$	n	K_n	$t_{0.5}$	n	K_n	$t_{0.5}$	n	K_n	$t_{0.5}$	n	K_n
125	246	1.8	6.6×10^{-6}	–	–	–	–	–	–	–	–	–
127	370	1.7	2.8×10^{-6}	198	1.9	1.0×10^{-5}	–	–	–	–	–	–
129	552	1.8	1.2×10^{-6}	337	1.9	3.4×10^{-6}	198	1.9	1.8×10^{-5}	–	–	–
131	1320	1.9	1.9×10^{-7}	528	2.1	1.3×10^{-6}	352	2.2	5.6×10^{-6}	140	2.8	3.0×10^{-6}
133	1860	2.4	9.4×10^{-8}	990	2.2	3.5×10^{-7}	492	1.9	4.3×10^{-6}	195	2.5	1.3×10^{-6}
135	2232	2.4	6.4×10^{-8}	1176	2.0	2.5×10^{-7}	740	2.0	1.3×10^{-6}	378	2.4	2.5×10^{-7}
137	3234	2.4	2.9×10^{-8}	1832	2.3	9.7×10^{-8}	1200	2.0	4.8×10^{-7}	773	2.7	4.2×10^{-8}
139	–	–	–	–	–	–	–	–	–	1155	2.5	1.5×10^{-8}
141	–	–	–	–	–	–	–	–	–	–	–	–
	IPP–iPP*-5			GRiPP–iPP*-6			GRiPP–iPP*-7			GRiPP–iPP*-8		
	$t_{0.5}$	n	K_n	$t_{0.5}$	n	K_n	$t_{0.5}$	n	K_n	$t_{0.5}$	n	K_n
	–	–	–	–	–	–	–	–	–	–	–	–
	–	–	–	–	–	–	–	–	–	–	–	–
	–	–	–	–	–	–	–	–	–	–	–	–
	–	–	–	–	–	–	–	–	–	–	–	–
	–	–	–	–	–	–	170	2.5	1.8×10^{-6}	205	2.3	6.8×10^{-7}
	233	2.0	1.4×10^{-6}	320	2.8	1.2×10^{-7}	269	2.4	5.8×10^{-7}	316	2.3	2.2×10^{-7}
	384	2.4	4.3×10^{-7}	490	2.7	3.8×10^{-8}	467	2.5	1.5×10^{-7}	562	2.7	4.9×10^{-8}
	580	2.6	1.6×10^{-7}	812	2.8	9.7×10^{-9}	670	2.4	6.0×10^{-8}	903	2.9	1.4×10^{-8}
	930	2.4	5.2×10^{-8}	1260	2.7	2.9×10^{-9}	1178	2.7	1.4×10^{-8}	1092	2.9	8.7×10^{-8}

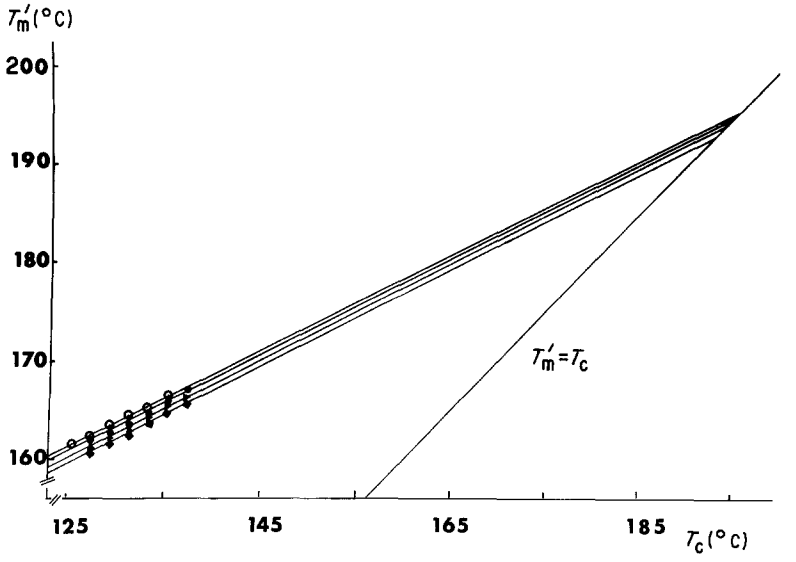

Figure 8 Variation of the melting temperature T'_m of (○) iPP-1, (●) GRiPP-2, (▲) GRiPP-3, (◆) GRiPP-4 with the crystallization temperature T_c. The extrapolation of the experimental points to the line $T'_m = T_c$ determined the value of the equilibrium melting temperature T_m of each sample.

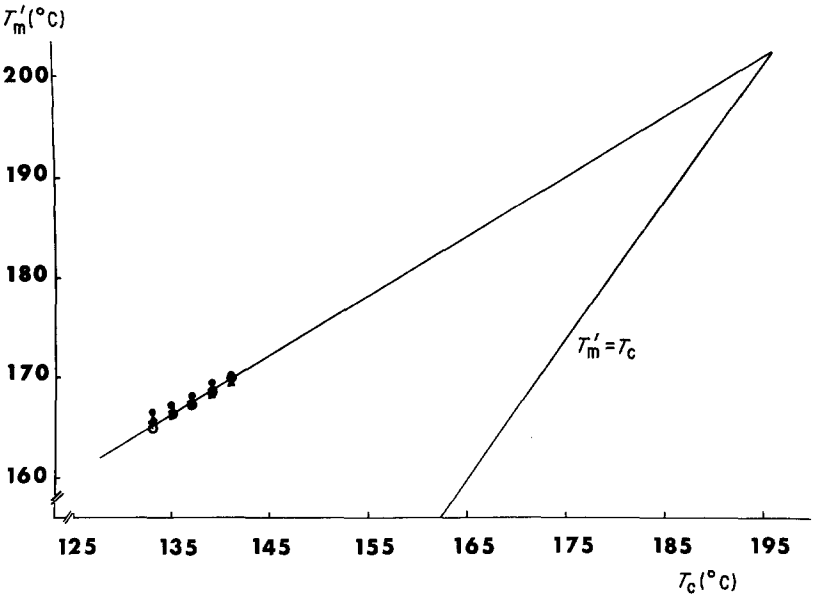

Figure 9 Variation of the melting temperature T'_m of (●) iPP–iPP*-5, (⊙) GRiPP–iPP*-6, (▲) GRiPP–iPP*-7, (■) GRiPP–iPP*-8 with T_c.

a process of coherent two-dimensional surface secondary nucleation, then, in accordance with the kinetic theory of polymer crystallization [8], the temperature dependence of K_n is given by the relation

$$\frac{1}{n}\log K_n = A_0 - \frac{\Delta F^*}{2.3RT_c} - \frac{\Delta\Phi^*}{2.3KT_c} \quad (5)$$

where A_0 is a constant (assuming that the density of primary nucleation at each T_c examined does not vary with time), ΔF^* is the activation energy for the transport of crystallizing units across the liquid–solid interface, and $\Delta\Phi^*$ is the energy of formation of a nucleus of critical dimensions expressed as

$$\Delta\Phi^* = \frac{4b_0\sigma\sigma_e T_m}{\Delta H_f \Delta T} \quad (6)$$

In Equation 6, b_0 is the distance between two adjacent fold planes, σ and σ_e are the free energy of formation per unit area of lateral and fold surfaces, respectively,

TABLE III Value of the equilibrium melting temperature T_m and constant γ for the various samples of iPP

Sample	T_m (K)	γ
iPP-1	469	2.0
GRiPP-2	469	2.0
GRiPP-3	468	2.0
GRiPP-4	467	1.9
iPP–iPP*-5	471	2.0
GRiPP–iPP*-6	471	1.9
GRiPP–iPP*-7	471	2.1
GRiPP–iPP*-8	471	2.0

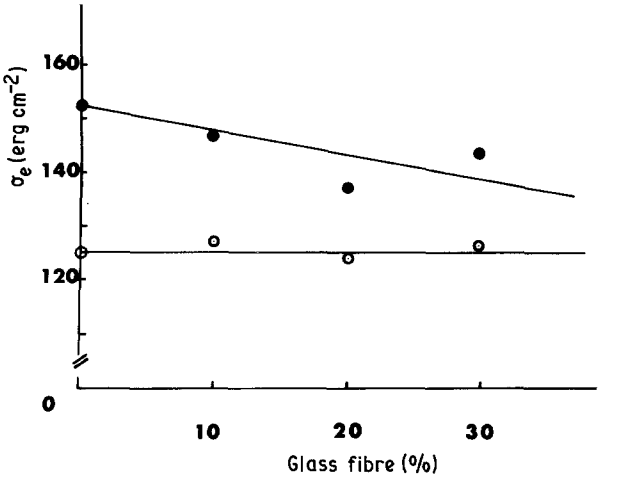

Figure 10 Surface free energy of folding σ_e as function of glass content: (●) GRiPP, (⊙) GRiPP–iPP*. 1 erg = 10^{-7} J.

TABLE IV Mechanical tests

Sample	Flexural elastic modulus (MPa) (ASTM D790)	Tensile strength at break (MPa) (ASTM D638)	Tensile elongation at break (%) (ASTM D638)	Izod impact strength at 20° C ($J\,m^{-1}$) (ASTM D256)	Heat distortion temperature (° C) (ASTM D648)	Rockwell hardness (ASTM D785)	Creep deflection measured after 8 h, weight = 100 $kg\,cm^{-2}$ (%)
iPP-1	1620	22.5	480	21	59	106	8.20
GRiPP-2	2680	56	3.2	74	148	111	1.20
GRiPP-3	4040	70	2.5	109	152	111	0.80
GRiPP-4	5720	74	2.0	83	152	111	0.55
iPP–iPP*-5	1640	22.5	345	17	60	107	6.00
GRiPP–iPP*-6	2740	58	3.3	57	151	112	1.10
GRiPP–iPP*-7	4160	77	3.0	92	152	112	0.70
GRiPP–iPP*-8	5630	91	2.5	95	155	112	0.40
NiPP-9	1950	28.5	20	19	65	108	5.00
GRNiPP-10	2820	57	3.2	86	151	111	1.12
GRNiPP-11	4200	67	2.2	74	151	111	0.75
GRNiPP-12	5670	70	1.5	79	154	111	0.48

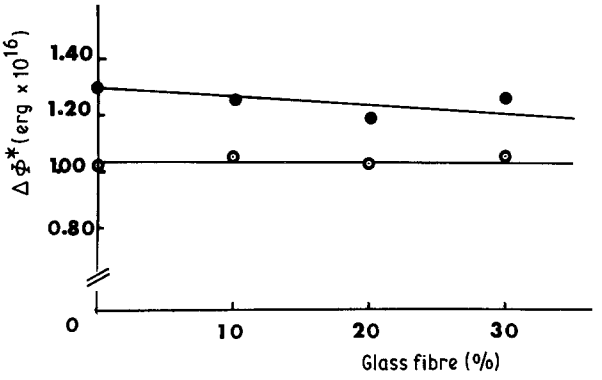

Figure 11 Free energy of formation of a nucleus of critical dimensions $\Delta\Phi^*$ against the glass content: (●) GRiPP (○) GRiPP–iPP*. T_c = 135° C.

ΔH_f is the enthalpy of fusion and ΔT ($= T_m - T_c$) is the undercooling.

The transport term ΔF^* is usually expressed as the activation energy of viscous flow according to the relation of Williams, Landel and Ferry [9]:

$$\Delta F^* = \frac{C_1 T_c}{C_2 + T_c - T_g} \tag{7}$$

where C_1 and C_2 are constants, generally assumed equal to 4.12 kcal mol^{-1} (17.2 kJ mol^{-1}) and 51.5 K, respectively, and T_g is the glass transition temperature. For all samples examined, T_g = 260 K was used according to the literature data [10].

Plots of $(1/n) \log K_n + \Delta F^*/2.3 RT_c$ against $T_m/T_c\Delta T$ are straight lines for all samples investigated. From the slopes of these lines the following quantity was determined:

$$\frac{4b_0\sigma\sigma_e}{2.3 K_n \Delta H_f} \tag{8}$$

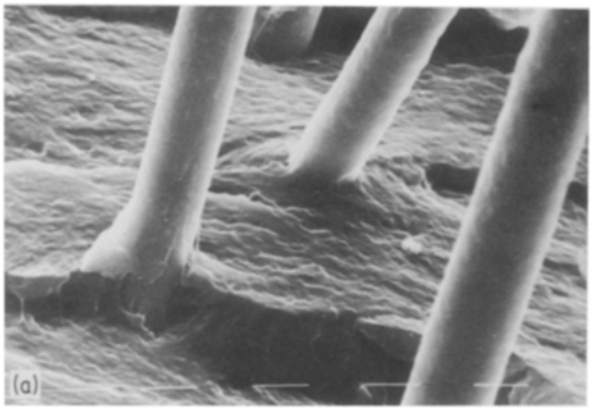

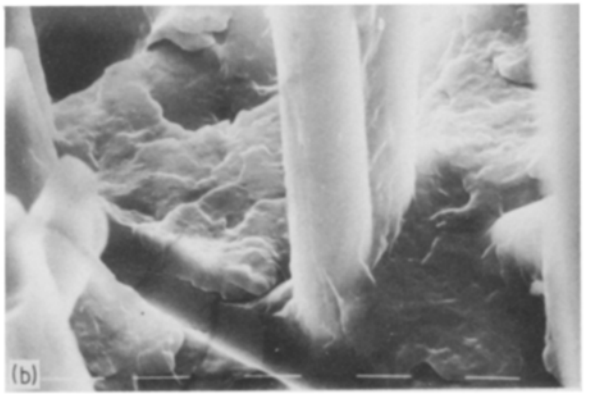

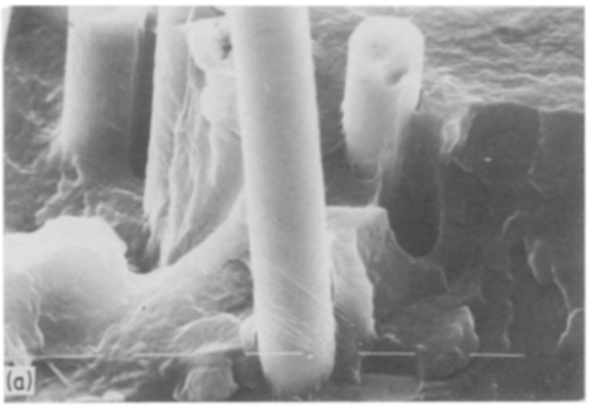

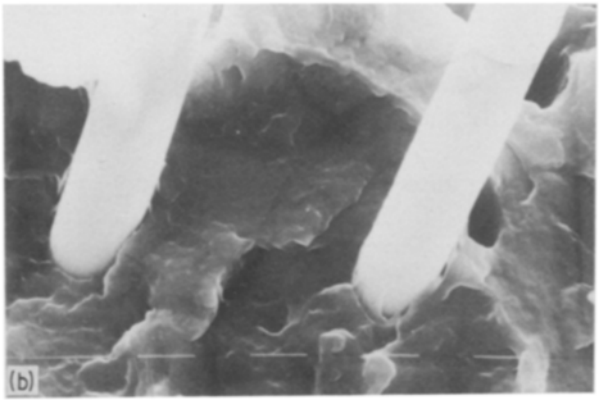

Figure 12 Electron micrographs of fractured surfaces of GRiPP samples: (a) GRiPP-3 (× 575), (b) GRiPP-4 (× 575).

Substituting in Equation 8 b_0 = 0.525 nm [10], ΔH_f = 209 kJ kg^{-1} [5] and σ = 0.1 $b_0\Delta H_f$, the surface energy of folding σ_e of iPP lamellar crystals and the free energy of formation of a nucleus of critical dimensions $\Delta\Phi^*$ were calculated. Plots of such quantities against the glass fibre content for Samples 1 to 8 are shown in Figs 10 and 11. From the figures it emerges that

(i) σ_e and $\Delta\Phi^*$ are almost independent of glass fibre content in the case of the composite containing iPP*, whereas for GRiPP samples both σ_e and $\Delta\Phi^*$ decrease with increasing glass fibre content.

(ii) both σ_e and $\Delta\Phi^*$ are systematically lower for iPP* containing composites.

Figure 13 Electron micrographs of fractured surfaces of GRiPP–iPP* samples: (a) GRiPP–iPP*-6 (× 575), (b) GRiPP–iPP*-7 (× 575), (c) GRiPP–iPP-8 (× 1150).

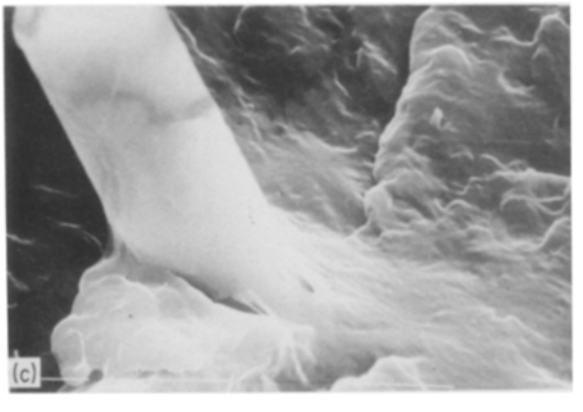

3.5. Mechanical properties

The results of mechanical tests for iPP, GRiPP, iPP–iPP*, GRiPP–iPP*, NiPP and GRNiPP samples are summarized in Table IV. It can be observed that in all cases the addition of fibres produces enhancement of the elastic modulus, the tensile strength, the Izod impact strength and the heat distortion temperature. On the other hand the elongation at break and the creep drastically decrease with an increase of the fibre content. Nevertheless it is interesting to point out that samples containing acrylic acid modified iPP* show values of the tensile strength and creep deflection comparatively better than those of iPP and NiPP samples, especially at higher fibre contents. Such behaviour is accounted for by the SEM observation of broken surfaces that show a better fibre–matrix adhesion in the case of GRiPP–iPP* samples (compare Figs 12 and 13).

The nucleation effect induced by the presence of iPP* in the samples could also play an important role in determining the mechanical response of the composites, even though the samples tested have been crystallized at very high undercooling. In such conditions of recrystallization even the plain iPP will crystallize according to a microspherulitic texture. The fact that in these samples the nucleation does not influence dramatically the mechanical response emerges from the values of the figures reported in Table IV.

Acknowledgement

This work was partly supported by Progetto Finalizzato "Chimica Fine e Secondaria" of CNR, Italy.

References

1. D. CAMPBELL and N. M. QAYYUUR, *J. Mater. Sci.* **12** (1977) 2427.
2. R. B. BURTON and M. S. FOLKER, *Plast. Rubb. Process. Appl.* **3** (1983) 129.
3. D. CAMPBELL and N. M. AQYYUUR, *J. Polym. Sci., Polym. Phys. Edn* **18** (1980) 83.
4. M. G. HUSON and W. S. McGILL, *ibid.* **23** (1985) 121.
5. S. BRANDUP and E. H. IMMERGUT, "Polymer Handbook" (Interscience, New York, 1975) Vol. 5, p. 24.
6. L. MANDELKEREN, "Crystallization Polymer" (McGraw-Hill, New York, 1964).
7. J. D. HOFFMAN, *Soc. Plast. Engrs Trans.* **4** (1964) 315.
8. J. D. HOFFMAN, G. T. DAVIS and S. I. LAURITZEN, in "Treatise on Solid State Chemistry", Vol. 3, edited by N. B. Hannay (Plenum, New York, 1976) Ch. 7.
9. H. L. WILLIAMS, R. F. LANDEL and J. D. S. FERRY, *J. Amer. Chem. Soc.* **77** (1955) 3701.
10. L. CRISPINO, E. MARTUSCELLI and M. PRACELLA, *Z. Makromol. Chem.* **181** (1980) 1747.

Received 23 September
and accepted 15 December 1986